JBC EDITORS' PICK

⌘ *Author's Choice*

The folding and unfolding behavior of ribonuclease H on the ribosome

Received for publication, April 15, 2020, and in revised form, June 4, 2020 Published, Papers in Press, June 11, 2020, DOI 10.1074/jbc.RA120.013909

Madeleine K. Jensen[1], **Avi J. Samelson**[1], **Annette Steward**[2], **Jane Clarke**[2], **and Susan Marqusee**[1,3,4,*]

From the [1]*Department of Molecular and Cell Biology, the* [3]*Institute for Quantitative Biosciences (QB3)–Berkeley, and the* [4]*Department of Chemistry, University of California, Berkeley, California, USA, and the* [2]*Department of Chemistry, University of Cambridge, Cambridge, United Kingdom*

Edited by Ursula Jakob

The health of a cell depends on accurate translation and proper protein folding, whereas misfolding can lead to aggregation and disease. The first opportunity for a protein to fold occurs during translation, when the ribosome and surrounding environment can affect the nascent chain energy landscape. However, quantifying these environmental effects is challenging because ribosomal proteins and rRNA preclude most spectroscopic measurements of protein energetics. Here, we have applied two gel-based approaches, pulse proteolysis and force-profile analysis, to probe the folding and unfolding pathways of RNase H (RNH) nascent chains stalled on the prokaryotic ribosome *in vitro*. We found that ribosome-stalled RNH has an increased unfolding rate compared with free RNH. Because protein stability is related to the ratio of the unfolding and folding rates, this increase completely accounts for the observed change in protein stability and indicates that the folding rate is unchanged. Using arrest peptide–based force-profile analysis, we assayed the force generated during the folding of RNH on the ribosome. Surprisingly, we found that population of the RNH folding intermediate is required to generate sufficient force to release a stall induced by the SecM stalling sequence and that read-through of SecM directly correlates with the stability of the RNH folding intermediate. Together, these results imply that the folding pathway of RNH is unchanged on the ribosome. Furthermore, our findings indicate that the ribosome promotes RNH unfolding while the nascent chain is proximal to the ribosome, which may limit the deleterious effects of RNH misfolding and assist in folding fidelity.

In the cell, a protein has its first opportunity to fold during synthesis on the ribosome. It is critical, therefore, that this initial folding event proceeds with fidelity and avoids toxic misfolded states (1, 2). Both the vectorial nature of translation and interactions with the ribosome can affect this process (3–8) such that the co-translational folding pathway can be different from the pathway observed during refolding experiments. For instance, co-translational folding of firefly luciferase promotes formation of an intermediate that helps to prevent misfolding (9). For the protein HaloTag, co-translational folding avoids an aggregation-prone intermediate and leads to more efficient folding (10). Both of these proteins have complex folding pathways, which include the formation of transient intermediates, and both show differences between their co-translational and refolding pathways. However, folding pathways are not necessarily altered by the ribosome; two small β-sheet domains, the src SH3 domain and titin I27, show simple two-state folding and appear to fold via the same pathway both on and off the ribosome (5, 11). Is populating transient folding intermediates required for folding to be modulated by the ribosome? To understand how proteins fold *in vivo*, it is essential to elucidate how the ribosome affects nascent chain folding.

Measuring the energetics and dynamics of ribosome-stalled nascent chains (RNCs) presents numerous experimental challenges. Historically, the kinetics of protein folding have been monitored with spectroscopic techniques, such as CD or fluorescence; structural features of the folding trajectory can be further probed by hydrogen-deuterium exchange (HDX) and by comparing stabilities and folding rates among site-specific variants of the protein of interest (ϕ-value analysis) (12). These well-established techniques, however, are not suitable for monitoring folding of an RNC; the ribosome contains over 50 proteins, which makes it impossible to specifically detect and measure folding of the nascent chain by most spectroscopic methods. Although more complex biophysical approaches, such as NMR (4, 6), FRET and photoinduced electron transfer (13, 14), and optical trap mechanical studies (3, 11, 15, 16), have elucidated important features of the folding process recently, these approaches are very technically challenging and have significant throughput limits. Thus, it is hard to know whether findings using these techniques are generally applicable to the entire proteome.

An alternative technique to measure folding kinetics and energetics in a complex mixture is pulse proteolysis. Under appropriate conditions, a short pulse of proteolysis degrades unfolded proteins, leaving the population of folded proteins intact. Unlike limited proteolysis, which reports on the relative proteolytic susceptibility of a protein, pulse proteolysis can be used to measure the fraction of folded protein in a given mixture quantitatively. Pulse proteolysis has been applied under equilibrium conditions to determine protein stability (ΔG_{unf}) or in a kinetic experiment to assess unfolding kinetics (k_{unf}) and

* For correspondence: Susan Marqusee, marqusee@berkeley.edu.

Present address for Avi J. Samelson: Dept. of Biochemistry and Biophysics, Institute for Neurodegenerative Diseases and California Institute for Quantitative Biomedical Research, University of California, San Francisco, California, USA.

requires very little protein relative to spectroscopic approaches (17–19). Because the fraction of folded protein is quantified by following a specific band on the gel, it can be carried out in complex mixtures, making it ideally suited for the study of RNCs.

We recently used pulse proteolysis to monitor the thermodynamic stability of proteins off and on the ribosome with varying linker lengths (or distances) from the peptidyl-transferase center (PTC) (20). For all proteins studied, the ribosome destabilizes nascent chains compared with free protein, and this destabilization depends on the distance from the PTC (20). The physical factors behind this destabilization remain unclear. Is the destabilization rooted in the folding and/or unfolding kinetics of the nascent chains? Pulse proteolysis applied to RNCs during a time course under nonequilibrium conditions can assess how the ribosome affects nascent chain folding and unfolding.

Another approach recently developed to explore the folding of RNCs is arrest peptide–based force-profile analysis (FPA) (21). FPA monitors the release of a stalled nascent chain, which has been shown to correlate with folding near the exit tunnel (5, 21–23) and has also been shown to be related to the global stability and folding topology of the nascent chain (24, 25). Despite several publications using this technique, details about the types of folding events required to release a stall are unclear. Release is usually attributed to global folding; however, force profiles of HemK and dihydrofolate reductase suggest that formation of an intermediate structure can also trigger release, resulting in bimodal or multimodal force profiles (23, 26).

Here, we apply pulse proteolysis to determine the unfolding rate of RNase H RNCs and combine this technique with FPA to understand how the ribosome modulates the folding and unfolding of RNase H (RNH). All work presented on RNH here refers to the cysteine-free variant (27, 28) that has been the subject of extensive studies in protein folding and stability. For ribosome-stalled RNH I53D (a two-state folding variant of RNH), the thermodynamic destabilization can be attributed to an increase in the unfolding rate, indicating that the folding rate is unaltered on the ribosome. Force-profile studies on two-state and three-state folding variants of RNH show that both the presence and the stability of the folding intermediate are critical for force generation and read-through of the stall sequence. Together, these results suggest that the folding pathway for RNH is the same on and off the ribosome and indicate that folding to a stable native state does not necessarily cause arrest-peptide release, whereas formation of a transiently populated intermediate is sufficient for release. These results have implications for understanding the fundamental principles of both co-translational folding and membrane protein translocation.

Results

Stability and kinetics of RNase H monitored by CD

The protein RNH has been extensively characterized in bulk by both CD and tryptophan fluorescence. The detail with which we understand its energy landscape make it a prime candidate for further studies on the ribosome (29, 30). These data, however, were all obtained in a buffered solution at pH 5.5, not the pH 7.4 buffer conditions (with divalent cations) required for on-the-ribosome studies. Therefore, we measured the stability and unfolding kinetics of RNH I53D by CD in a buffer that both more closely approximates physiological conditions and is suitable for ribosome-bound experiments (pH 7.4, 150 mM KCl, 15 mM $Mg(OAc)_2$, 0.1 mM tris(2-carboxyethyl)phosphine). Compared with the previous studies at pH 5.5, RNH I53D is slightly destabilized (ΔG_{unf} = 4.71 ± 0.32 kcal/mol *versus* 5.6 ± 0.4 kcal/mol) (Fig. 1*A* and Table 1). The extrapolated unfolding rate in the absence of denaturant is slightly higher (2.0 (± 0.5) × 10^{-5} s^{-1} at pH 7.4 compared with 6.3 (± 5) × 10^{-6} s^{-1} at pH 5.5) (Fig. 1*B* and Table 1), and $m^{\ddagger}_{unf}$ = 0.45 ± 0.02 kcal mol^{-1} M^{-1} at pH 7.4, within error of the $m^{\ddagger}_{unf}$ measured previously for RNH I53D (0.5 ± 0.1 kcal mol^{-1} M^{-1}, pH 5.5) (29). These data serve as a point of comparison for the gel-based studies comparing folding on and off the ribosome.

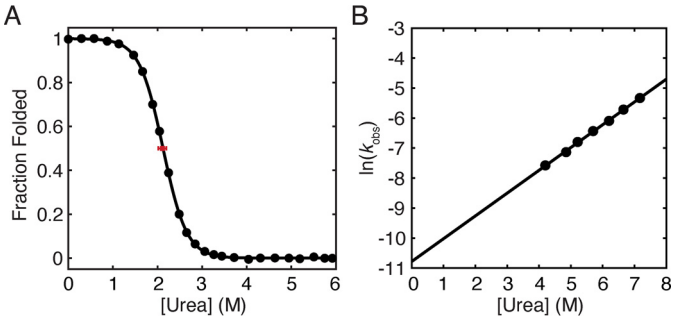

Figure 1. Stability and unfolding kinetics of RNH I53D measured by CD at pH 7.4. *A*, equilibrium urea-induced denaturant melt (*black circles*) of RNH I53D (pH 7.4 at 25 °C). The data were fit using a two-state approximation (U ⇌ N, where U and N are the unfolded and native states, respectively), and the data shown are from one representative experiment of three. The average C_m from three experiments is marked by a *red square* with an *error bar* for the S.D. *B*, natural log of the observed unfolding rate for RNH I53D at pH 7.4 as a function of urea.

Ribosome-tethered RNH I53D has a higher unfolding rate than free protein

Previous pulse proteolysis studies determined the equilibrium stability (ΔG_{unf}) of RNH I53D on and off the ribosome (20). The observed destabilization on the ribosome implies an underlying change in the folding and/or unfolding kinetics. If the two-state folding mechanism of RNH I53D holds true as an RNC, measurements of the unfolding rate via pulse proteolysis will allow us to infer changes in the folding rate ($K_{eq} = k_{unf}/k_{fold}$).

Unfolding kinetics were monitored using pulse proteolysis by rapidly diluting a protein or RNC sample to a specific final urea concentration and following the fraction folded as a function of time by assaying with a pulse of thermolysin-based proteolysis (see "Experimental procedures"). Nascent chains with a C-terminal 10-residue glycine-serine (GS) linker and the well-characterized SecM stalling sequence were tagged by incorporating BODIPY-FL-$Lysine^{AAA}$-tRNA (Promega) during *in vitro* transcription/translation (IVT) (20) (Fig. 2*A*; see also "Experimental procedures"). Our pulse length of 1 min allows us to measure unfolding rates on the order of ~10^{-2} s^{-1} or less, which partially dictates the urea concentrations accessible for

Table 1
Stability and unfolding kinetics of RNH I53D

	RNH I53D (CD)	RNH I53D-$(GS)_5$-SecM	
		Off	On
C_m (M, urea)	2.11 ± 0.09	2.14 ± 0.13[a]	1.65 ± 0.10[a]
ΔG_{unf} (kcal/mol)	4.71 ± 0.32	4.77 ± 0.29[b]	3.68 ± 0.22[b]
m_{unf} (kcal mol^{-1} M^{-1})	2.23 ± 0.06		
$k_{unf}^{0M\ urea}$ (s^{-1})	2.0 (± 0.5) × 10^{-5}	4.6 (± 2. 6) × 10^{-5}	3.8 × 10^{-4} ± 1.0 × 10^{-3}
$m_{unf}^{\ddagger}$ (kcal mol^{-1} M^{-1})	0.45 ± 0.02	0.34 ± 0.09	0.43 ± 0.65

[a] The values are from Samelson *et al.* (20); pH 7.4 buffer with divalent cations.
[b] The values were calculated using m_{unf} from CD.

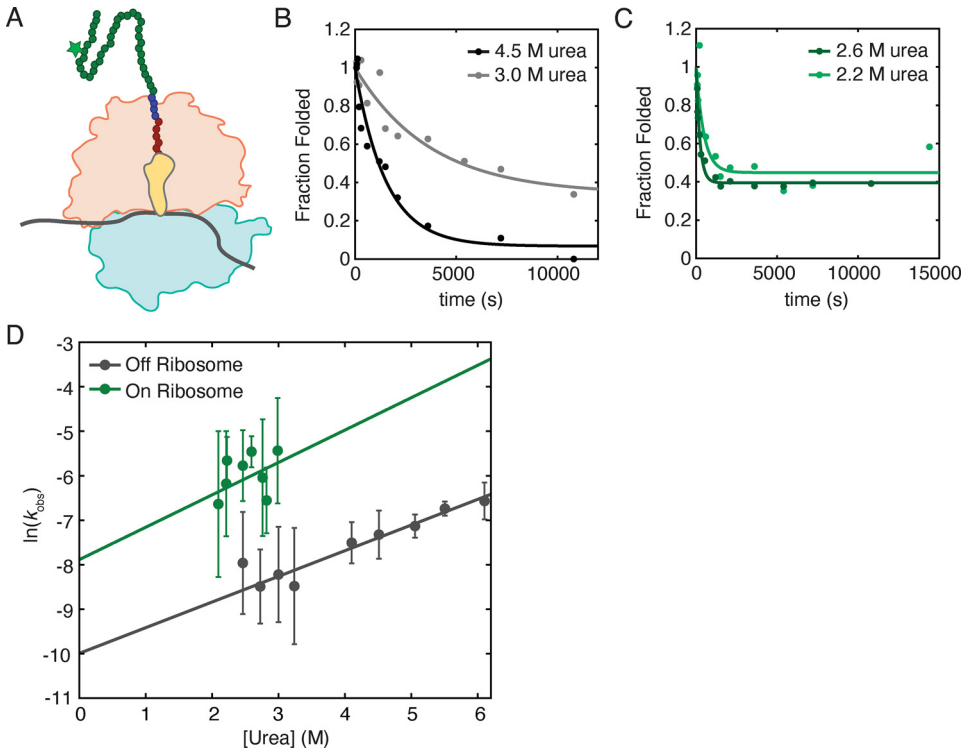

Figure 2. Unfolding kinetics as measured by pulse proteolysis. *A*, cartoon representation of a ribosome-stalled nascent chain generated for pulse proteolysis experiments. A 50S subunit (*orange*) and 30S subunit (*light blue*) with a peptidyl-tRNA (*yellow*) stalls during translation of mRNA (*gray*) at a SecM stall sequence (*red circles*). The protein of interest (*green circles*) is extended beyond the ribosome exit tunnel by a 10-residue glycine–serine linker (*blue circles*). The nascent chain is tagged with a BODIPY-FL-Lysine (*star*). *B*, representative traces of observed off-ribosome unfolding rates of RNH I53D at 4.5 M urea (*black*) and 3.0 M urea (*gray*). *C*, representative traces of observed on-ribosome unfolding rates of RNH I53D at 2.6 M urea (*dark green*) and 2.2 M urea (*light green*). *D*, data sets including *B* and *C* are fit to a single exponential to extract k_{obs}, and the ln(k_{obs}) for experiments on (*green*) and off the ribosome (*gray*) are plotted at several urea concentrations. *Error bars* are the 95% confidence interval of the fits to a single exponential at each urea concentration. These data are fit to a linear model weighted for the error at each point where the slope is $m_{unf}^{\ddagger}$, and the *y* intercept is $k_{unf}^{0M\ urea}$, the unfolding rate in a 0 M denaturant condition. The urea concentrations at which we can investigate the unfolding rates of nascent chains are limited based on the C_m of the nascent chain and the stability of 70S ribosomes, leading to a higher error for the extrapolation of on-ribosome data.

these measurements. For studies on RNCs, the experiments were also limited to below 3.5 M urea to maintain the integrity of the ribosome, which dissociates above 3.5 M urea (20). Although the observed unfolding rates are reproducible across experiments, the final amplitudes of these kinetic traces vary and cannot be directly compared with equilibrium pulse proteolysis and CD data (Fig. 2, *B* and *C*).

Off the ribosome, RNH I53D-$(GS)_5$-SecM unfolds with $k_{unf}^{0M\ urea}$ = 4.6 (± 2.6) × 10^{-5} s^{-1} and $m_{unf}^{\ddagger}$ = 0.34 ± 0.09 kcal mol^{-1} M^{-1} (Fig. 2, *B* and *D*, and Table 1), within error of that determined by CD (Table 1). On the ribosome, we measured $k_{unf}^{0M\ urea}$ to be 3.8 × 10^{-4} s^{-1} ± 1.0 × 10^{-3}, an order of magnitude greater than off the ribosome (Fig. 2, *C* and *D*, and Table 1). The $m^{\ddagger}$ values are comparable on and off the ribosome, with $m_{unf}^{\ddagger}$ = 0.43 ± 0.65 kcal mol^{-1} M^{-1} for the RNC (Fig. 2*D* and Table 1). Assuming that RNH I53D is two-state on the ribosome, k_{fold} = 0.2 s^{-1}, similar to that obtained by pulse proteolysis off the ribosome (k_{fold} = 0.1 s^{-1}, pH 7.4) and from bulk CD experiments (0.1 s^{-1}, pH 5.5) (29).

RNH I53D does not read through the SecM stall

The folding trajectory of ribosome-bound nascent chains can be interrogated directly using arrest peptide–based force-profile analysis (23). Arrest peptides, such as the SecM stalling sequence, are highly sensitive to tension on the nascent chain, and tension generated because of folding has been shown to release arrest (5, 21–23, 26). FPA measures the fraction

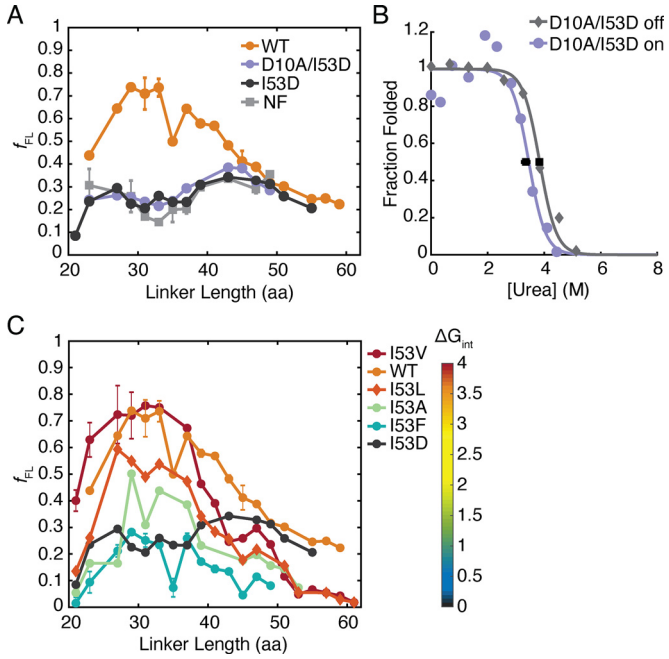

Figure 3. Force-profile analysis of RNH variants. *A*, FPA of RNH WT (*orange circles*), a NF control (*light gray squares*), which is RNH F8A/I25A/I53D/W85A, RNH I53D (*dark gray circles*), and RNH D10A/I53D (*purple circles*). The *lines* connect the data to show trends and are not fits. Where "L##" denotes a linker length, the following are the averages of two experiments: WT L23, L27, L31, L33, L35, L37, L39, L43, and L45; NF L29, L31, L33, L35, L43. NF L23, L27, L37, L39, and L47 are the averages of three experiments. All other points shown are the results of a single experiment. *Error bars* shown are S. D. *B*, stability of RNH D10A/I53D-$(GS)_5$-SecM measured off (*gray diamonds*) and on (*purple circles*) the ribosome by pulse proteolysis from IVT-produced (PURExpress ΔRF123) protein. The data shown are representative of three experiments off and two experiments on the ribosome with *black squares* marking the average C_m values from on and off the ribosome samples and *error bars* showing the S. D. The data are fit using a two-state approximation. *C*, FPA of RNH I53 variants: I53V (*red circles*), I53L (*orange diamonds*), I53A (*green circles*), and I53F (*blue circles*). WT (*orange circles*) and RNH I53D (*gray circles*) are repeated from *A* for reference. The heat map shows the color coding of the variants based on the stability of their folding intermediate (ΔG_{int}). The *lines* connect the data to show trends and are not fits. I53V L21, L23, L27, and L29, as well as I53F L21, L23, L27, L29, L31, L33, L35, L37, L39, and L41, are the averages of two experiments with the S. D. shown as *error bars*. All other points are the result of single experiments.

readthrough of the SecM stall (f_{FL}) as a function of linker length between the protein of interest and the PTC. At each linker length, the f_{FL} is a readout of the fraction of nascent chains that release the stall. The connection between the biophysical properties of the nascent chain and the f_{FL} remains unclear. The stability of the nascent chain, its topology, and its folding rate have all been linked to the amplitude of the f_{FL} (24, 25). Thus, a comparison of FPA on the well-characterized protein RNH with the on-ribosome energetics and kinetics obtained by pulse proteolysis should help to decipher these effects, in addition to reporting on the RNH folding trajectory on the ribosome.

Fig. 3*A* shows the force profiles of both RNH I53D and a nonfolding control. Four mutations were needed to generate the nonfolding control (F8A/I25A/I53D/W85A) based on data derived from bulk ensemble studies on variants of RNH and assumed additivity (29, 31, 32). As expected, the nonfolding variant shows minimal release of the stall sequence across all linker lengths tested (Fig. 3*A*). Surprisingly, the force-profile assay for RNH I53D resembles the nonfolding variant (Fig. 3*A*). This result is not due to a lack of the ability of RNH I53D to fold on the ribosome because pulse proteolysis data confirm that RNH I53D can fold on the ribosome with a 35-residue linker (20). Importantly, the calculated on-ribosome k_{fold} indicates that RNH I53D-$(GS)_5$-SecM has ample time to fold during FPA, where samples are incubated for 15 min prior to measuring release (see above). Despite this, folding does not appear to generate the force needed for release of the SecM-mediated stall.

Three-state RNH can read through SecM stall

To determine whether this uncoupling of folding and SecM readthrough holds for other RNases H, we then turned to WT RNH, which is known to fold in a three-state manner ($U \rightleftharpoons I \rightleftharpoons N$, where U, I, and N are the unfolded, intermediate, and native states, respectively) both in bulk and in single-molecule optical trap experiments (29, 33). In bulk ensemble studies, RNH is also more stable than RNH I53D (ΔG_{unf} = 9.7 *versus* 5.6 kcal/mol, pH 5.5) (29, 34). Fig. 3*A* shows that the force profile of RNH is notably different than those observed for RNH I53D and the nonfolding control. Unlike the others, RNH shows significant release ($f_{FL} > 0.5$) occurring at linker lengths from 29 to 41 residues. Thus, RNH folding is capable of generating the force necessary to release the stall.

Increased global stability does not result in SecM readthrough

We made a stabilizing variant of RNH I53D, RNH D10A/I53D, which has a stability near that of WT RNH (ΔG_{unf} = 8.5 kcal/mol, pH 5.5) and, like RNH I53D, shows two-state folding in bulk studies (32). This construct would allow us to distinguish whether SecM readthrough is failing because of global stability or population of the intermediate. The off-ribosome stability of RNH D10A/I53D-$(GS)_5$-SecM is 7.66 ± 0.03 kcal/mol *versus* 6.71 ± 0.28 kcal/mol as a stalled nascent chain (Fig. 3*B* and Table 2). Both are significantly more stable than RNH I53D. Despite its increased stability, this variant also failed to release the stall at all linker lengths (Fig. 3*A*). Thus, the release observed for RNH is not solely because of its high stability. This suggests that it is either the formation of the RNase H folding intermediate or the process of folding from the intermediate that is responsible for force generation on the SecM stall sequence.

Stability of the folding intermediate correlates with arrest peptide release

To test the role of the kinetic folding intermediate in force generation and release of the stall, we turned to a series of site-specific variants known to modulate the stability of the intermediate. The folding intermediate of RNH has been well-characterized by pulse-labeling HDX and protein engineering (32, 35, 36). Residue 53 resides in the center of helix A, an important structural feature of the intermediate. Altering the hydrophobicity and size of residue 53 is known to modulate both the stability of the intermediate (ΔG_{int}, the difference in free energy between U and I) and global stability of the protein (ΔG_{unf}) (29). These site-specific variants range from near-WT ΔG_{int} (RNH I53V and RNH I53L) to no detectable intermediate (two-state folding) for RNH I53D (Table 3). To examine the effect of

Table 2
Stability of RNH D10A/I53D. The off-ribosome values are from three experiments, and the on-ribosome values are from two experiments

		RNH D10A/I53D-$(GS)_5$-SecM	
	RNH D10A/I53D (CD)[a]	Off	On
C_m (M, urea)	4.25 ± 0.2	3.83 ± 0.02	3.35 ± 0.14
ΔG_{unf} (kcal/mol)	8.5 ± 0.4	7.66 ± 0.03	6.71 ± 0.28
m_{unf} (kcal mol^{-1} M^{-1})	2.0 ± 0.1		

[a] The values are from Connell *et al.* (32); pH 5.5 buffer without divalent cations.

Table 3
Kinetic folding parameters for RNH I53 variants. Kinetic folding parameters for RNH I53 variants measured by Spudich *et al.* (29); pH 5.5 buffer without divalent cations

	RNH	RNH I53V	RNH I53L	RNH I53A	RNH I53F
ΔG_{unf} (kcal/mol)	9.9	10.6	9.0	8	6.3
m_{unf} (kcal mol^{-1} M^{-1})	2.1	2.3	2.3	2.4	2.2
ΔG_{int} (kcal/mol)	3.5	4.0	3.6	1.7	0.8

these mutations on the force profile of RNH, we generated four additional substitutions (Val, Leu, Ala, and Phe) at residue 53 for 20 linker lengths ranging from 21 to 61 residues.

The stability of the intermediate appears to play the dominant role in determining the force profile. For all five variants at position 53, a higher ΔG_{int} leads to more robust readthrough of the SecM stalling sequence. RNH I53V and RNH I53L, which have near-WT ΔG_{unf} and ΔG_{int}, have WT-like force profiles in terms of the linker lengths at which significant amounts of full-length protein are produced and the overall broadness of the peaks (Fig. 3*C*). RNH I53A, for which ΔG_{int} = 1.7 kcal/mol at pH 5.5 (29, 34), did not generate more than 50% f_{FL} at any linker length despite its high global stability, ΔG_{unf} = 8 kcal/mol (Fig. 3*C*). Likewise, RNH I53F barely populates the intermediate (ΔG_{int} = 0.8 kcal/mol) (29), and readthrough of SecM was not notably different from the force profile of RNH I53D.

Discussion

We have used a combination of pulse proteolysis and arrest peptide–based force-profile experiments to investigate how the ribosome modulates folding and unfolding of the small protein RNase H. For RNH I53D-$(GS)_5$-SecM, we observed an increase in the unfolding rate on the ribosome of approximately an order of magnitude compared with off the ribosome at all urea concentrations tested. This accounts for the observed decrease in stability for these RNCs. Although we can only sample a limited range of urea concentrations in these RNC experiments, the similarity in urea dependence ($m^{\ddagger}_{unf}$) indicates that the protein is traversing the same transition-state barrier on and off the ribosome, consistent with observations for the small proteins titin and SH3 (5, 11). Assuming that RNH I53D folds in a two-state mechanism on the ribosome (populating only U and N), this implies that the presence of the ribosome does not affect the folding rate and suggests a mechanism by which the ribosome destabilizes the nascent chain by promoting its unfolding. In general, such increases in the unfolding rate could provide a mechanism for delayed folding of the emerging nascent chain until it has extended far enough from the PTC to avoid nonnative, toxic states.

Despite its robust folding as an RNC, our studies suggest that the folding of RNH I53D does not generate enough force to read through the SecM stall in FPA. Our pulse proteolysis studies allow us to measure both the stability and unfolding rate for RNH I53D-$(GS)_5$-SecM, indicating that RNH I53D is capable of folding on the ribosome with a linker of 35 amino acids from the PTC. However, in our force-profile assays, RNH I53D does not read through the SecM stall at any linker length from 21 to 61 residues. Therefore, stable folding cannot be the only requirement for force generation in the force-profile assays. Moreover, increasing global stability for this protein, such as in RNH D10A/I53D, also does not result in an increase in f_{FL}. Previous studies have interpreted the release of translation arrest during FPA as nascent chain folding and, inversely, lack of release as either a lack of folding or folding that occurs far from the ribosome surface (5, 21–23). Our results demonstrate that stable folding alone does not trigger SecM readthrough.

However, several other variants of RNH do show appreciable force-generated release, all of which are known to populate an early intermediate in the refolding trajectory. WT RNH releases and reads through the SecM stall for a broad range of linker lengths. Additionally, by studying a series of site-specific variants, we find that ΔG_{int} is directly related to the f_{FL} produced. Compared with RNH, the f_{FL} diminishes with decreasing ΔG_{int} for these variants, showing that we can tune the release of RNH by adjusting the stability of the intermediate. In agreement with previous studies, the amplitude of f_{FL} for these three-state variants correlates with global stability (24, 25). Because the stability of the intermediate is related to the height of the subsequent folding barrier, this kinetic barrier may play a role. Interestingly, we observe release of three-state RNH variants at lower linker lengths than would be expected based solely on the relationship between protein length and the linker length of maximum f_{FL} (24). Perhaps the topology of RNH is important for this release at low linker lengths (25). Additionally, the discrepancy could be explained by release being initiated by folding of the intermediate, which contains 79 residues as compared with the 155 residues of the full-length protein. Together, our data suggest that a baseline global stability and population of the folding intermediate are required for RNH to generate sufficient force to release a SecM stall and indicate that FPA is more nuanced than simply reporting on folding to the native state.

The correlation between the three-state and two-state folding of variants in standard refolding experiments and their ability to read through the SecM stall implies that the intermediate observed in CD and HDX studies off the ribosome is likely populated on the ribosome and again suggests that the general folding trajectory, or pathway, of RNH is unaltered on the ribosome. These data, together with the pulse proteolysis results, agree with studies of the folding mechanisms of other small proteins on the ribosome that have shown that the folding trajectory does not change for RNCs relative to free proteins (5, 11). Combining this pulse proteolysis approach with other site-specific mutations in a ϕ-value analysis will further elucidate the folding pathway of ribosome-tethered RNH I53D and could be applied to other nascent chains to characterize the effect of the ribosome on a range of folding mechanisms.

Our results suggest that the transient folding intermediate of RNase H is responsible for generating the tension required to release the SecM stall. This is perhaps not surprising given that the intermediate of RNH has a stability comparable to many globular proteins and similar to the small zinc-binding peptide used in the development of FPA (21). Notably, the stability of the intermediate is quite low, suggesting that a stability of just 1–2 kcal/mol is enough to induce release. Perhaps more surprising, however, is that a stable variant of RNH without this kinetic intermediate is incapable of release.

What properties of the folding of RNH I53D prevent the formation of force sufficient to cause release? Perhaps the answer lies in the kinetics of folding. The two-state variants of RNH are known to fold significantly slower than the three-state variants—the same regions that stabilize the kinetic intermediate are involved in the rate-limiting step, or transition state, for folding (35). Previous bulk experiments have shown that RNH I53D folds at a rate approximately four times lower than RNH. From our pulse-proteolysis experiments, we infer an off-ribosome folding rate of 0.1 s^{-1} for RNH I53D, relative to k_{fold} = 0.74 s^{-1} for RNH off the ribosome in bulk CD experiments (29). These questions might be best answered by simulations, which can dissect the mechanism of force generation (5, 11, 25).

In addition to the specific results we find for RNH, the approaches used here (equilibrium and kinetic pulse proteolysis, together with FPA) are a start to a detailed quantitative comparison of protein folding on and off the ribosome, which will lead to a better understanding of protein folding in the cell. FPA has already been used to examine the role of chaperones, such as trigger factor, in the folding of nascent chains (26). Future work can look toward pairing these quantitative experiments with structural studies, such as HDX, to elucidate the folding trajectory in complex, cellular-like environments and could eventually be expanded to investigate the influence of the vectorial and kinetic aspects of translation.

Experimental procedures

Generation of plasmids for pulse proteolysis

The coding sequence for RNH I53D was cloned into the dihydrofolate reductase control template provided by New England Biolabs with the PURExpress kit via NdeI and KpnI restriction sites. GS linkers and a SecM stalling sequence with an N-terminal extension (EFLPYRQFSTPVWISQAQGIRAGPQ) were added to the C terminus of the RNH I53D coding sequence by around-the-horn mutagenesis (20, 37). RNH D10A/I53D constructs were generated by subsequent around-the-horn mutagenesis. All constructs were verified by sequencing.

Preparation of samples for pulse proteolysis

Using PURExpress kits (New England Biolabs), 37.5-μl IVT reactions were assembled on ice with 1.5 μl of RNase inhibitor, murine (New England Biolabs), 2 μl of FluoroTect GreenLys (Promega), and 375 ng of plasmid encoding the protein of interest. Standard PURExpress kits (E6800S) were used to produce off-ribosome samples, and PURExpress ΔRF123 kits (E6850S) were used to generate RNCs in the absence of release factors. IVT reactions were incubated at 37 °C for 45 min to 2 h.

Pulse proteolysis

To monitor off-ribosome kinetics, we treated the samples with RNase A before carrying out pulse proteolysis. RNase A (Sigma–Aldrich) was added to IVT reactions at a final concentration of 1 mg/ml and incubated for 15–30 min at 37 °C. These reactions were diluted to 65 μl in 1 × HKMT (25 mM HEPES, pH 7.4, 15 mM $Mg(OAc)_2$, 150 mM KCl, 0.1 mM tris(2-carboxyethyl)phosphine). For on-ribosome samples, stalled RNCs were pelleted by ultracentrifugation on a 94 μl, 1 M sucrose cushion in 1× HKMT for 40 min at 200,000 × *g*. The pellet was washed twice with 100 μl of 1× HKMT and resuspended in 65 μl of 1× HKMT. Measurements of stability by pulse proteolysis were performed as previously described (20). To measure unfolding kinetics, urea stock solutions were set up such that dilution with 49.5 μl of either free protein or RNCs would result in the desired final urea concentration in 1× HKMT. The sample to be tested was rapidly diluted into the urea stock and pipetted up and down to mix, and for each time point, 10 μl was removed and pulsed into a tube containing 1 μl of 2 mg/ml thermolysin (Sigma–Aldrich) for 1 min before quenching with 3 μl of 500 mM EDTA, pH 8.5.

On-ribosome samples were incubated in 1 mg/ml RNase A after pulse proteolysis for 15–30 min at 37 °C. Samples were mixed with SDS-PAGE loading dye, loaded onto 4–12% or 12% NuPAGE Bis-Tris gels (Thermo Fisher), and run in MES buffer for 50 min at 170 V at 4 °C. A full-length RNH marker was run to aid in quantification. The gels were imaged on a Typhoon FLA9500 (GE Healthcare) with a 488-nm laser and a 510LP filter. Analysis of band intensities was performed as described previously using ImageJ (20). All urea concentrations were determined after the dilution with RNCs or released protein by refractometer, as previously (18).

CD stability and unfolding kinetics

The plasmid for RNH I53D was constructed previously (29) and was expressed and purified from inclusion bodies as previously described (36). The data were recorded on an Aviv 430 CD spectropolarimeter at 225 nm and 25 °C in a 0.5-cm pathlength cuvette in 1× HKMT buffer. All urea concentrations were determined by refractometer. Equilibrium denaturation experiments were performed after incubating protein

samples overnight at the appropriate urea concentrations. The samples were stirred for 60 s prior to measurement, and data were recorded for 60 s and averaged for each urea concentration. Unfolding kinetics were initiated by rapidly mixing a 100 μM stock of RNH I53D at 0.2 M urea 1:3 (v/v) in 1× HKMT and the appropriate urea concentration to reach a final denaturant concentration of 4–8 M urea. The samples were manually mixed, and dead-times ranged from 15 to 20 s. The dead-time was added to the start of each trace before fitting. All data were plotted and fit using MatLab as described previously (29).

Cloning for force-profile constructs

The RNH coding sequence was inserted into a pRSETA plasmid containing fragments of LepB and a SecM stalling sequence under the control of a T7 promoter as described previously (38). This created a set of pRSETA plasmids containing RNH with 20 different linker lengths from the RNH C terminus to the SecM stall sequence. Linker lengths ranged from 21 to 61 residues. Variants of RNH were made by around-the-horn mutagenesis on this set of 20 plasmids. All constructs were verified by sequencing.

Force-profile analysis

RNCs tethered with varying linker lengths will range in the tension induced on the SecM stall sequence during folding. A very short linker will inhibit protein folding because of occlusion of a portion of the protein in the exit tunnel or interactions between the ribosome and the nascent chain. Extending the linker will allow the protein to fold, and the tension generated will be proportional to the fraction of nascent chains that release the SecM stalling sequence (f_{FL}). At longer linker lengths, protein folding is distant from the PTC, and there is no coupling between folding and the stall sequence.

RNCs were generated using standard PURExpress kits (New England Biolabs). A 240-μl IVT master mix was assembled on ice, containing 10 μl of RNase inhibitor, murine (New England Biolabs), and 12 μl of either EasyTag EXPRESS^{35}S protein labeling mix (PerkinElmer) or L-[^{35}S] Met (PerkinElmer). For each sample, 9 μl of this master mix was added to 1 μl of plasmid DNA (~250 ng/μl) and incubated at 37 °C for exactly 15 min before quenching with 1 μl of 10 mg/ml RNase A and 1 μl of 20 mM chloramphenicol. The samples were incubated at 37 °C for an additional 15 min, mixed with 3 μl of 4× LDS loading dye (New England Biolabs), and loaded onto 4–12% NuPAGE Bis-Tris gels (Thermo Fisher). The gels were run in MES buffer for 75 min at 150 V at room temperature.

Analysis of force-profile data

Gel band intensities were determined by plotting the signal intensity for a cross-section of each lane in ImageJ. The data were fit to a bimodal Gaussian distribution in MatLab to calculate f_{FL} using the following equations,

$$\text{Signal intensity} = A + Be^{\frac{-(X-C)^2}{2D^2}} + Ee^{\frac{-(X-F)^2}{2G^2}} \quad \text{(Eq. 1)}$$

$$I_{FL} = BD\sqrt{2\pi} \quad \text{(Eq. 2)}$$

$$I_A = EG\sqrt{2\pi} \quad \text{(Eq. 3)}$$

$$f_{FL} = I_{FL}/(I_{FL} + I_A) \quad \text{(Eq. 4)}$$

where I_{FL} is the intensity of the full-length band, and I_A is the intensity of the stalled band.

The following f_{FL} were calculated as the average of two experiments: WT L23, L27, L31, L33, L35, L37, L39, L43, L45; NF L29, L31, L33, L35, and L43; I53V L21, L23, L27, and L29; and I53F L21, L23, L27, L29, L31, L33, L35, L37, L39, and L41. NF L23, L27, L37, L39, and L47 are the averages of three experiments. All other f_{FL} shown are the result of a single experiment. The experiment is robust and has been shown to be highly reproducible (5, 22).

Data availability

All data are contained within the article.

Acknowledgments—We thank Brendan Maguire for cloning ~150 variants of RNH and different linker lengths for the force-profile work and for helping to purify proteins for CD. We also thank Liang Ming Wee, Lisa Alexander, and Guillermo Chacaltana for guidance and workspace use for the force-profile experiments and the members of the Marqusee Lab for insights and feedback. We are grateful to Robert Best and Pengfei Tian for work on simulations and fruitful discussions.

Author contributions—M. K. J., A. J. S., J. C., and S. M. conceptualization; M. K. J., A. J. S., and AS data curation; M. K. J., A. J. S., and AS formal analysis; M. K. J., J. C., and S. M. funding acquisition; M. K. J., A. J. S., and AS investigation; M. K. J. visualization; M. K. J., A. J. S., and AS methodology; M. K. J. and S. M. writing-original draft; M. K. J., A. J. S., AS, J. C., and S. M. writing-review and editing; S. M. supervision; S. M. project administration.

Funding and additional information—This work was supported by National Institutes of Health Grant R01-GM050945 (to S. M.) and National Science Foundation Graduate Research Fellowships Program Grant DGE1106400 (to M. K. J.). S. M. is a Chan Zuckerberg Biohub Investigator. This work is also supported by Wellcome Trust Grant WT095195 (to J. C.). J. C. is a Wellcome Trust Senior Research Fellow. The content is solely the responsibility of the authors and does not necessarily represent the official views of the National Institutes of Health.

Conflict of interest—The authors declare that they have no conflicts of interest with the contents of this article.

Abbreviations—The abbreviations used are: RNC, ribosome-stalled nascent chains; RNH, RNase H; HDX, hydrogen–deuterium exchange; PTC, peptidyl-transferase center; FPA, force-profile analysis; GS, glycine–serine; IVT, *in vitro* transcription/translation; NF, nonfolding.

References

1. Dobson, C. M. (1999) Protein misfolding, evolution and disease. *Trends Biochem. Sci.* **24,** 329–332 CrossRef Medline

2. Hipp, M. S., Park, S. H., and Hartl, U. U. (2014) Proteostasis impairment in protein-misfolding and -aggregation diseases. *Trends Cell Biol.* **24,** 506–514 CrossRef Medline
3. Kaiser, C. M., Goldman, D. H., Chodera, J. D., Tinoco, I., and Bustamante, C. (2011) The ribosome modulates nascent protein folding. *Science* **334,** 1723–1727 CrossRef Medline
4. Waudby, C. A., Wlodarski, T., Karyadi, M.-E., Cassaignau, A. M. E., Chan, S. H. S., Wentink, A. S., Schmidt-Engler, J. M., Camilloni, C., Vendruscolo, M., Cabrita, L. D., and Christodoulou, J. (2018) Systematic mapping of free energy landscapes of a growing filamin domain during biosynthesis. *Proc. Natl. Acad. Sci. U.S.A.* **115,** 9744–9749 CrossRef Medline
5. Tian, P., Steward, A., Kudva, R., Su, T., Shilling, P. J., Nickson, A. A., Hollins, J. J., Beckmann, R., von Heijne, G., Clarke, J., and Best, R. B. (2018) Folding pathway of an Ig domain is conserved on and off the ribosome. *Proc. Natl. Acad. Sci. U.S.A.* **115,** E11284–E11293 CrossRef Medline
6. Deckert, A., Waudby, C. A., Wlodarski, T., Wentink, A. S., Wang, X., Kirkpatrick, J. P., Paton, J. F. S., Camilloni, C., Kukic, P., Dobson, C. M., Vendruscolo, M., Cabrita, L. D., and Christodoulou, J. (2016) Structural characterization of the interaction of α-synuclein nascent chains with the ribosomal surface and trigger factor. *Proc. Natl. Acad. Sci. U.S.A.* **113,** 5012–5017 CrossRef Medline
7. Sander, I. M., Chaney, J. L., and Clark, P. L. (2014) Expanding Anfinsen's principle: contributions of synonymous codon selection to rational protein design. *J. Am. Chem. Soc.* **136,** 858–861 CrossRef Medline
8. Clark, P. L. (2004) Protein folding in the cell: reshaping the folding funnel. *Trends Biochem. Sci.* **29,** 527–534 CrossRef Medline
9. Frydman, J., Erdjument-Bromage, H., Tempst, P., and Hartl, F. U. (1999) Co-translational domain folding as the structural basis for the rapid de novo folding of firefly luciferase. *Nat. Struct. Biol.* **6,** 697–705 CrossRef Medline
10. Samelson, A. J., Bolin, E., Costello, S. M., Sharma, A. K., O'Brien, E. P., and Marqusee, S. (2018) Kinetic and structural comparison of a protein's cotranslational folding and refolding pathways. *Sci. Adv.* **4,** eaas9098 CrossRef Medline
11. Guinn, E. J., Tian, P., Shin, M., Best, R. B., and Marqusee, S. (2018) A small single-domain protein folds through the same pathway on and off the ribosome. *Proc. Natl. Acad. Sci. U.S.A.* **115,** 12206–12211 CrossRef Medline
12. Ozkan, S. B., Bahar, I., and Dill, K. A. (2001) Transition states and the meaning of Φ-values in protein folding kinetics. *Nat. Struct. Biol.* **8,** 765–769 CrossRef Medline
13. Holtkamp, W., Kokic, G., Jäger, M., Mittelstaet, J., Komar, A. A., and Rodnina, M. V. (2015) Cotranslational protein folding on the ribosome monitored in real time. *Science* **350,** 1104–1107 CrossRef Medline
14. Mercier, E., and Rodnina, M. V. (2018) Co-translational folding trajectory of the HemK helical domain. *Biochemistry* **57,** 3460–3464 CrossRef Medline
15. Goldman, D. H., Kaiser, C. M., Milin, A., Righini, M., Tinoco, I., and Bustamante, C. (2015) Mechanical force releases nascent chain–mediated ribosome arrest *in vitro* and *in vivo*. *Science* **348,** 457–460 CrossRef Medline
16. Liu, K., Rehfus, J. E., Mattson, E., and Kaiser, C. M. (2017) The ribosome destabilizes native and non-native structures in a nascent multidomain protein. *Protein Sci.* **26,** 1439–1451 CrossRef Medline
17. Park, C., and Marqusee, S. (2006) Quantitative determination of protein stability and ligand binding by pulse proteolysis. *Curr. Protoc. Protein Sci.* Chapter 20, Unit 10.11 Medline
18. Park, C., and Marqusee, S. (2005) Pulse proteolysis: A simple method for quantitative determination of protein stability and ligand binding. *Nat. Methods* **2,** 207–212 CrossRef Medline
19. Na, Y.-R., and Park, C. (2009) Investigating protein unfolding kinetics by pulse proteolysis. *Protein Sci.* **18,** 268–276 CrossRef Medline
20. Samelson, A. J., Jensen, M. K., Soto, R. A., Cate, J. H. D., and Marqusee, S. (2016) Quantitative determination of ribosome nascent chain stability. *Proc. Natl. Acad. Sci. U.S.A.* **113,** 13402–13407 CrossRef Medline
21. Nilsson, O. B., Hedman, R., Marino, J., Wickles, S., Bischoff, L., Johansson, M., Müller-Lucks, A., Trovato, F., Puglisi, J. D., O'Brien, E. P., Beckmann, R., and von Heijne, G. (2015) Cotranslational protein folding inside the ribosome exit tunnel. *Cell Rep.* **12,** 1533–1540 CrossRef Medline
22. Nilsson, O. B., Nickson, A. A., Hollins, J. J., Wickles, S., Steward, A., Beckmann, R., von Heijne, G., and Clarke, J. (2017) Cotranslational folding of spectrin domains via partially structured states. *Nat. Struct. Mol. Biol.* **24,** 221–225 CrossRef Medline
23. Kemp, G., Kudva, R., de la Rosa, A., and von Heijne, G. (2019) Force-profile analysis of the cotranslational folding of HemK and filamin domains: comparison of biochemical and biophysical folding assays. *J. Mol. Biol.* **431,** 1308–1314 CrossRef Medline
24. Farías-Rico, J. A., Ruud Selin, F., Myronidi, I., Frühauf, M., and von Heijne, G. (2018) Effects of protein size, thermodynamic stability, and net charge on cotranslational folding on the ribosome. *Proc. Natl. Acad. Sci. U.S.A.* **115,** E9280–E9287 CrossRef Medline
25. Leininger, S. E., Trovato, F., Nissley, D. A., and O'Brien, E. P. (2019) Domain topology, stability, and translation speed determine mechanical force generation on the ribosome. *Proc. Natl. Acad. Sci. U.S.A.* **116,** 5523–5532 CrossRef Medline
26. Nilsson, O. B., Müller-Lucks, A., Kramer, G., Bukau, B., and Von Heijne, G. (2016) Trigger factor reduces the force exerted on the nascent chain by a cotranslationally folding protein. *J. Mol. Biol.* **428,** 1356–1364 CrossRef Medline
27. Dabora, J. M., and Marqusee, S. (1994) Equilibrium unfolding of *Escherichia coli* ribonuclease H: characterization of a partially folded state. *Protein Sci.* **3,** 1401–1408 CrossRef Medline
28. Kanaya, S., Kimura, S., Katsuda, C., and Ikehara, M. (1990) Role of cysteine residues in ribonuclease H from Escherichia coli. Site-directed mutagenesis and chemical modification. *Biochem. J.* **271,** 59–66 CrossRef Medline
29. Spudich, G. M., Miller, E. J., and Marqusee, S. (2004) Destabilization of the *Escherichia coli* RNase H kinetic intermediate: switching between a two-state and three-state folding mechanism. *J. Mol. Biol.* **335,** 609–618 CrossRef Medline
30. Rosen, L. E., Kathuria, S. V., Matthews, C. R., Bilsel, O., and Marqusee, S. (2015) Non-native structure appears in microseconds during the folding of *E. coli* RNase H. *J. Mol. Biol.* **427,** 443–453 CrossRef Medline
31. Connell, K. B., Horner, G. A., and Marqusee, S. (2009) A single mutation at residue 25 populates the folding intermediate of *E. coli* RNase H and reveals a highly dynamic partially folded ensemble. *J. Mol. Biol.* **391,** 461–470 CrossRef Medline
32. Connell, K. B., Miller, E. J., and Marqusee, S. (2009) The folding trajectory of RNase H is dominated by its topology and not local stability: a protein engineering study of variants that fold via two-state and three-state mechanisms. *J. Mol. Biol.* **391,** 450–460 CrossRef Medline
33. Cecconi, C., Shank, E. A., Bustamante, C., and Marqusee, S. (2005) Direct observation of the three-state of a single protein molecule. *Science* **309,** 2057–2060 CrossRef Medline
34. Raschke, T. M., Kho, J., and Marqusee, S. (1999) Confirmation of the hierarchical folding of RNase H: a protein engineering study. *Nat. Struct. Biol.* **6,** 825–831 CrossRef Medline
35. Hu, W., Walters, B. T., Kan, Z., Mayne, L., Rosen, L. E., Marqusee, S., and Englander, S. W. (2013) Stepwise protein folding at near amino acid resolution by hydrogen exchange and mass spectrometry. *Proc. Natl. Acad. Sci. U.S.A.* **110,** 7684–7689 CrossRef Medline
36. Rosen, L. E., Connell, K. B., and Marqusee, S. (2014) Evidence for close side-chain packing in an early protein folding intermediate previously assumed to be a molten globule. *Proc. Natl. Acad. Sci. U.S.A.* **111,** 14746–14751 CrossRef Medline
37. Floor, S. (2018) *Around-the-horn PCR and cloning. protocols.io*. CrossRef
38. Ismail, N., Hedman, R., Schiller, N., and Von Heijne, G. (2012) A biphasic pulling force acts on transmembrane helices during translocon-mediated membrane integration. *Nat. Struct. Mol. Biol.* **19,** 1018–1023 CrossRef Medline